HHS Public Access

Author manuscript

Med Sci Sports Exerc. Author manuscript; available in PMC 2017 July 01.

Published in final edited form as:

Med Sci Sports Exerc. 2016 July ; 48(7): 1259–1269. doi:10.1249/MSS.0000000000000898.

Ovariectomized High Fit Rats Are Protected against Diet-Induced Insulin Resistance

Young-Min Park[1], **Jill A. Kanaley**[1], **Terese M. Zidon**[1], **Rebecca J. Welly**[1], **Rebecca J. Scroggins**[1], **Steven L. Britton**[2], **Lauren G. Koch**[2], **John P. Thyfault**[3], **Frank W. Booth**[4], **Jaume Padilla**[1,5,6], and **Victoria J. Vieira-Potter**[1]

[1]Nutrition and Exercise Physiology, University of Missouri, Columbia, MO

[2]Department of Anesthesiology, University of Michigan Medical School, Ann Arbor, MI

[3]Department of Molecular Integrative Physiology, University of Kansas Medical Center, Kansas City, KS

[4]Biomedical Sciences, University of Missouri, Columbia, MO

[5]Child Health, University of Missouri, Columbia, MO

[6]Dalton Cardiovascular Research Center, University of Missouri, Columbia, MO

Abstract

Introduction—In the absence of exercise training, rats selectively bred for high intrinsic aerobic capacity (HCR) are protected against ovariectomy (OVX)-induced insulin resistance and obesity compared to those bred for low intrinsic aerobic capacity (LCR).

Purpose—This study determined whether OVX HCR rats remain protected with exposure to high fat diet (HFD) compared to OVX LCR rats.

Methods—Female HCR and LCR rats (n=36; age 27-33 weeks) underwent OVX and were randomized to a standard chow diet (NC; 5% kcal fat) or HFD (45% kcal fat), *ad libitum* for 11 weeks. Total energy expenditure (TEE), resting energy expenditure (REE), spontaneous physical activity (SPA), and glucose tolerance were assessed midway, while fasting circulating metabolic markers, body composition, adipose tissue distribution, and skeletal muscle AMPK and mitochondrial markers were assessed at sacrifice.

Results—Both HCR and LCR experienced HFD-induced increases in total and visceral adiposity following OVX. Despite similar gains in adiposity, HCR rats were protected from HFD-induced insulin resistance and reduced TEE observed in LCR rats ($P<0.05$). This metabolic protection was likely attributed to a compensatory increase in SPA and associated preservation of skeletal muscle AMPK activity in HCR; whereas, HFD significantly reduced SPA and AMPK activity in LCR ($P<0.05$). In both lines, HFD reduced citrate synthase activity, gene expression of markers of

Correspondence: Victoria J. Vieira-Potter, Assistant Professor, vieirapotterv@missouri.edu 573 882 2027 (Ph), Department of Nutrition and Exercise Physiology, 204 Gwynn Hall, University of Missouri, Columbia, MO 65211.

Conflict of Interest: None. The results of the present study do not constitute endorsement by ACSM.

mitochondrial biogenesis (tFAM, NRF1, and PGC-1α), and protein levels of mitochondrial oxidative phosphorylation complexes I, II, IV, and V in skeletal muscle (all $P<0.05$).

Conclusion—Following OVX, HCR and LCR rats differentially respond to HFD such that HCR increase while LCR decrease SPA. This "physical activity compensation" likely confers protection from HFD-induced insulin resistance and reduced energy expenditure in HCR rats.

Keywords

estrogen loss; ovariectomy; exercise; spontaneous physical activity; skeletal muscle metabolism; energy expenditure

Introduction

Reduced physical activity is known to decrease aerobic fitness (1), and low aerobic fitness is a strong, independent risk factor for metabolic disease and all-cause mortality (16). Further, considerable evidence suggests that impaired aerobic capacity and skeletal muscle mitochondrial function are strongly linked to whole body insulin resistance (13). Conversely, increased physical activity and exercise training can reverse or attenuate the prevalence of cardiovascular disease, metabolic syndrome, and type 2 diabetes (T2D) in individuals with metabolic dysfunction (16, 21). In a dose-dependent fashion, exercise training-related improvements in aerobic fitness associate significantly with improvements in metabolic syndrome-related markers (5). While exercise training and increased aerobic fitness are closely linked and have long been associated with attenuated morbidity and mortality, the unique impact of inherent aerobic fitness, and the metabolic mechanisms responsible for this protection, remain largely unknown.

A growing body of literature using a rat model of contrasting aerobic fitness (i.e. high-capacity running (HCR) and low-capacity running (LCR) rats) has demonstrated a robust protective role of aerobic fitness on a multitude of metabolic outcomes (25-27, 33, 37, 39, 40). Naples et al. (26) demonstrated that female HCR rats had greater skeletal muscle mitochondrial function assessed by free fatty acid oxidation and cytochrome c protein, compared to LCR rats, and HCR rats were inherently more insulin sensitive compared to LCR rats (40). Recent studies further substantiated the findings that skeletal muscle mitochondrial oxidative capacity is greater in HCR than LCR (33), and that HCR were protected against high fat diet (HFD)-induced hepatic steatosis (25). Noteworthy is that increased basal skeletal muscle oxidative capacity has been shown to protect HCR rats from HFD-induced insulin resistance and obesity (26, 27). Yet, it is unknown if this protective effect, driven by high oxidative capacity, against HFD-induced insulin resistance and obesity would persist even following ovariectomy (OVX), a model of ovarian hormone depletion.

OVX in rodents models human menopause in that they develop metabolic dysfunction and obesity. Previous research has shown that ovary-intact female HCR rats are resistant to HFD-induced metabolic dysfunction and obesity (26, 27). Recently, our group demonstrated that HCR rats are also impervious to early OVX-induced insulin resistance and the accretion of adiposity, extending the protective role of aerobic fitness to the OVX condition (39). That study, however, raised some important questions. Unexpectedly, the protection against OVX-

related insulin resistance and obesity observed in female HCR rats showed no association with skeletal muscle mitochondrial markers. Specifically, OVX had no impact on mitochondrial biogenesis markers (i.e. gene and protein content of skeletal muscle PGC-1α and oxidative phosphorylation subunits). OVX also unexpectedly increased a marker of mitochondrial content (i.e. citrate synthase enzyme activity) in skeletal muscle similarly in HCR and LCR rats, perhaps indicative of a compensatory effect (39). These findings suggest that the role of skeletal muscle mitochondrial biogenesis and content may not be critical in the protection against OVX-induced insulin resistance and obesity in HCR rats.

In the present study, HCR_{OVX} and LCR_{OVX} rats were challenged with HFD versus normal chow diet to determine if high aerobic fitness is protective against HFD-induced metabolic dysfunction and impairments in skeletal muscle mitochondrial markers following OVX. Since HFD is known to adversely affect skeletal muscle mitochondrial function (35), we reasoned that the greater mitochondrial function in HCR rats, even after OVX, would protect them from metabolic impairments. Therefore, the purpose of the present study was to address the hypotheses that: 1) OVX rats bred for greater aerobic capacity (i.e. HCR) are protected from HFD-induced obesity and insulin resistance; and 2) an underlying mechanism by which HCR_{OVX} rats are protected from HFD-induced metabolic dysfunction is preservation of skeletal muscle mitochondrial biogenesis and content.

Methods

Animals

The HCR/LCR rat model has been well characterized (15, 25-27, 37). Thirty six randomly-cycling female HCR and LCR rats from generation 32 were tested for running capacity at the University of Michigan at approximately 11 weeks of age, and then shipped to the University of Missouri at approximately 20 weeks of age, where the rats were acclimated for the next 10 weeks. Rats were singly housed under standard humidity and temperature on a 12h-12h light/dark cycle, and fed standard rodent chow (Harlan Teklad Rodent Diet 8604) and water *ad libitum* until surgeries and group randomization. All animal procedures were approved by Institutional Animal Care and Use Committee (IACUC) at the University of Missouri-Columbia.

Experimental design

When rats were ∼30 weeks old (age range: 27-33 weeks), all were OVX. Following a 1-week recovery period, during which time all rats were single-housed, they were randomized either to remain on normal rodent chow (NC - 5% kcal fat, 8604, Harlan Teklad) or switch to high fat diet (HFD - 45% kcal fat, D12451, Research Diets) generating 4 groups: HCR_{NC} (n=8), HCR_{HFD} (n=7), LCR_{NC} (n=14), and LCR_{HFD} (n=7). All were fed *ad libitum* for 11 weeks. At week 6 following OVX, intraperitoneal glucose tolerance tests (GTT), with measurement of glucose-mediated insulin response, were conducted as an assessment of insulin sensitivity. At week 9 following OVX, food intake was assessed (over one week) and expressed as $kcal \cdot day^{-1} \cdot BWg^{-1}$. Total energy expenditure (TEE), resting energy expenditure (REE), respiratory quotient (RQ), and cage spontaneous physical activity (SPA) were measured one week prior to sacrifice. These measurements were not all performed together

at the end of the study for logistical reasons, but the time course with which the experiments were performed was the same for all animals. We wanted to ensure that all animals fully recovered from any stress that may have been induced by the *in vivo* experiments prior to sacrifice, so that all final fasting blood measures were collected during neuroendocrine homeostasis. Moreover, performing GTT midway and measuring fasting glucose and insulin at sacrifice gave us some indication about how the animals responded to HFD over time. On the day of sacrifice, body composition was measured via dual energy x-ray absorptiometry (DXA; Hologic QDR-1000, calibrated for rodents), and tissues and plasma samples were collected, immediately snap frozen in liquid nitrogen, and stored at -80 °C until analysis.

Ovariectomy surgeries

OVX surgeries were performed as previously described (12). Briefly, rats were anesthetized with inhaled isoflurane which was kept at 2% during surgery. A 2.5 cm incision at midline of the dorsal surface was made, followed by two bilateral incisions through the muscle layer to expose the ovaries. Following ovary removal, the skin incision was closed using wound clips, and acetaminophen (500 $mg \cdot kg^{-1}$) was administered.

Metabolic monitoring and spontaneous physical activity assessment

Using a metabolic monitoring system (Promethion, Sable Systems Int., Las Vegas, NV), TEE, REE, and RQ were determined via indirect calorimetry (i.e., by monitoring oxygen consumption and carbon dioxide production over a 72-h period as previously described (39)). Thirty minutes of the lowest REE were selected to calculate 24-hour REE. Both TEE and REE were calculated relative to body weight. SPA is assessed via quantification of a three-dimensional series of infrared beams (X+Y+Z) and expressed this way (i.e., an assessment that includes animal rearing) as well as two-dimensionally (i.e., an assessment of back and forth, front to back movement without rearing). Prior to data collection, animals were singly housed in the metabolic chamber and acclimated to the chamber environment for one day. Data were analyzed as cycle averages (i.e. 12-hour light and dark cycle averages) and calculated per animal; individual animal averages were then used to determine group means.

Intraperitoneal glucose tolerance tests

Following an overnight fast, baseline blood samples were collected from the tail vein using a 23 g × 3/4 inch blood collection set (Terumo Medical Corp., Somerset, NJ). A sterile glucose solution (2 $g \cdot kg\ BW^{-1}$) was injected into the peritoneum. Blood glucose concentrations were measured at 15, 30, 45, 60, and 120 minutes using a hand-held rodent glucometer (AlphaTrak, Abbott Labs, Abbot Park, IL). Insulin concentration was assessed from plasma collected at each GTT time point using rat insulin ELISA kits via manufacturer's instructions (Alpco Corp., Salem, NH). The parameter calculated for glucose and insulin is the total area under the curve (tAUC) from baseline to 120 min time point. The Matsuda index was used to calculate insulin sensitivity during GTT (22).

Circulating metabolic markers

On the day of sacrifice, 8-hour fasted rats were anesthetized with sodium pentobarbital (100 $mg \cdot kg^{-1}$). Blood samples were collected via cardiac puncture into 2.0 mL EDTA-treated microcentrifuge tubes (Fisher scientific, Pittsburgh, PA) and plasma was collected by centrifugation using an Eppendorf 5702R centrifuge at 3,000 rpm for 15 min at 4°C. Plasma was immediately stored at -80°C until analysis. Hemolyzed plasma samples were excluded from analysis. Fasting insulin, glucose, triglycerides (TG), non-esterified fatty acids (NEFA), high-density lipoprotein (HDL), and low-density lipoprotein (LDL) concentrations were determined using a clinical diagnostic service provided by the University of Missouri (Clinical Pathology Services, LLC) which employed commercially available assays according to manufacturer's guidelines, with an Olympus AU680 automated chemistry analyzer (Beckman-Coulter, Brea CA). The homeostasis model assessment of insulin resistance (HOMA-IR) and adipocyte-insulin resistance were used as a surrogate measure of insulin resistance (23). The formula of HOMA-IR index was fasting insulin × fasting glucose, with insulin and glucose values in $pg \cdot ml^{-1}$ and $mg \cdot dl^{-1}$, respectively. The formula of adipocyte-IR index was fasting insulin × fasting NEFA, with insulin and NEFA values in $pg \cdot ml^{-1}$ and $mmol \cdot l^{-1}$, respectively.

Body composition assessment

Body weight was measured weekly throughout the study. At the end of the study, body composition (i.e. total, fat and lean mass) was determined using DXA. Following DXA assessments, rats were sacrificed and fat distribution assessed via fat pad weights. Perigonadal, perirenal, and omental white adipose tissue (WAT), as well as interscapular brown adipose tissue (BAT) depots were removed and weighed to the nearest 0.01g as performed previously (29). Whole liver and heart were also collected, weighed, snap frozen and stored. In order to determine relative BAT, total BAT mass was expressed relative to WAT which was assessed as the sum of perigonadal, perirenal, and omental depots.

RNA extraction and real-time PCR

Whole gastrocnemius skeletal muscle tissue was pulverized and homogenized in TRIzol solution using a tissue homogenizer (TissueLyser LT, Qiagen, Valencia, CA). Total RNA was isolated using the Qiagen's RNeasy fibrous tissue protocol and measured using a Nanodrop spectrophotometer (Thermo Scientific, Wilmington, DE) to determine RNA purity and concentration. A subset of RNA samples were assessed for integrity via RNA fragment analysis; RQN values were all >8.0 with a mean value of 9.11 ± 0.42. cDNA was synthesized from total RNA using the High Capacity cDNA Reverse Transcription kit (Applied Biosystems, Carlsbad, CA). Quantitative real-time PCR was conducted using the ABI StepOne Plus sequence detection system (Applied Biosystems), as previously referenced by our group (29). Primer sequences were designed using the NCBI Primer Design tool, and all primers were purchased from IDT (Coralville, IA). A 20-μl reaction mixture containing the appropriate concentrations of gene-specific primers plus 4 μl of cDNA template, and 10 μl iTaq UniverSYBR Green SMX (BioRad, Hercules, CA) was loaded in each well of a 96-well plate in duplicate. The thermal conditions for PCR were 95°C for 10 min, followed by 40 cycles of 95°C for 15 s and 60°C for 45 sec. The specificity

of the PCR products was determined by a dissociation melt curve analysis. 18S primer was used to amplify the endogenous control product (i.e. HK gene). mRNA expression values are presented as $2^{\Delta CT}$ (ΔCT = HK CT - gene of interest CT). Each mRNA data was normalized to the HCR NC group, which was always expressed as 1.

SDS-PAGE western blot analysis

Western blotting was performed as previously referenced (37). Whole gastrocnemius skeletal muscle was pulverized and homogenized in Triton X-100 solution containing protease and phosphatase inhibitors using a tissue homogenizer (TissueLyser LT, Qiagen, Valencia, CA). Total protein value was determined using the Thermo Scientific Pierce BCA protein assay kit (Thermo Scientific, Rockford, IL). Samples containing the protein homogenates (40 ug of protein) and laemmli buffer were separated by SDS-PAGE, transferred to polyvinylidene difluoride (PVDF) membranes, and were probed with primary antibodies (1:1000 concentration in 5% bovine serum albumin). Oxidative phosphorylation (OX PHOS) complexes antibody containing complex I subunit NDUFB8, complex II-30kDa, complex IV subunit I, and complex V alpha subunit was purchased from Abcam (ab110413, Abcam, Cambridge, MA), and total adenosine monophosphate-activated protein kinase (AMPK)-α, pAMPK Thr^{172} (activation site) and (B) pAMPK $Ser^{485/491}$ (inhibition site) antibodies from Cell Signaling (#2532, #2531, and #4185, respectively; Beverly, MA). Individual protein bands were quantified using a densitometer (Bio-Rad), and normalized to β-Actin antibody (#4967, Abcam, Cambridge, MA).

Citrate synthase enzyme activity

Citrate synthase (CS) activity was determined by the experimental method of Srere et al. (36). Briefly, frozen gastrocnemius was pulverized and homogenized in Triton X-100 solution using a tissue homogenizer (TissueLyser LT, Qiagen, Valencia, CA). Homogenates were incubated in the presence of 10.0 mM oxaloacetate, 3.0 mM acetyl-CoA, and 1.0 mM 5,5′-dithiobis-2-nitrobenzoic (DTNB). An index of CS enzyme activity was determined using spectrophotometric assessment of reduced DTNB at a wavelength of 412 nm.

Statistical analysis

Statistical differences were analyzed using a 2 × 2 ANOVA to determine if differences existed between line (HCR vs. LCR), diet (NC vs. HFD), and whether diet × line interactions occurred for body composition, TEE, REE, SPA, RQ, food intake, circulating metabolic markers, HOMA-IR, adipocyte-IR, glucose/insulin responses during GTTs, uterine, and skeletal muscle AMPK activity, OX PHOS complexes, CS activity, and mitochondrial biogenesis mRNA expressions. When a significant line by diet interaction existed, LSD post-hoc test was used for pair-wise comparisons. For body weight gain over time, two-way ANOVA with repeated measures was used. All data were analyzed using SPSS 22.0. In all cases, $P<0.05$ was considered statistically different; data are reported as mean ± SEM.

Results

Animal characteristics and body composition

Initial body weight was ~20% higher in LCR rats compared to HCR rats (line main effect, $P<0.001$; Figure 1A). Throughout the study, HCR rats weighed less than LCR rats (time × line interaction, $P=0.003$). Both HCR and LCR rats experienced HFD-induced weight gain (diet main effect, $P<0.001$; Figure 1B); no line × diet interaction was observed. Both lines increased %fat following HFD (diet main effect, $P=0.006$; Figure 1C), and LCR rats had greater %fat than HCR rats (line main effect, $P<0.001$; Figure 1C). The major visceral depot, the perigonadal depot, increased following HFD in both lines, and LCR had greater perigonadal depot than HCR (Figure 1D; diet main effect, P=0.003; line main effect, P<0.001). Other visceral WAT depots (i.e. perirenal and omental) were also heavier in LCR than HCR rats (line main effect, $P<0.001$ and $P<0.007$, respectively), but HFD did not significantly increase these depots. All uteri were weighed post-mortem as indication of successful OVX surgeries. Our previous study using the same rat lines demonstrated that OVX resulted in ~73% uterine atrophy (P<0.001 compared to SHM), resulting in mean uterine mass of 0.30 ± 0.04 and 0.26 ± 0.03 g for HCR_{OVX} and LCR_{OVX}, respectively (39). The mean uterine mass of the OVX rats in this current study did not differ from those values (Table 1). However, circulating levels of estradiol were not measured which may be viewed as a potential limitation.

Energy expenditure and spontaneous physical activity

HCR rats showed greater total energy expenditure (TEE) than LCR rats in dark and light cycles (line main effect, $P<0.001$ in both cycles; Figure 2A). HFD reduced TEE in LCR but not HCR in a dark cycle (diet main effect, $P=0.008$; line × diet interaction, $P=0.025$; Figure 2A). Remarkably, this preservation of TEE in HCR rats appeared to be due to an HFD-induced increase in SPA, such that HCR rats *increased* and LCR *decreased* SPA following HFD (line × diet interaction, $P=0.003$, Figure 2B). SPA was greater in HCR than in LCR rats in both cycles (line main effect, $P<0.001$ in both cycles). In both cycles, resting energy expenditure (REE) was reduced similarly following HFD in both lines (diet main effect; dark $P=0.007$, light $P=0.024$; Figure 2C), and overall HCR rats had greater REE compared to LCR rats (line main effect, $P<0.001$ in both cycles). Covarying TEE and REE for body weight did not change our results. TEE was positively correlated with SPA (r=0.759, $P<0.0001$). There was no significant difference between groups in food intake relative to body weight (Figure 2D), while absolute food intake was greater in LCR than HCR (line main effect, $P=0.005$). Respiratory quotient (RQ) was reduced following HFD similarly in HCR and LCR suggesting an HFD-mediated increase in fat oxidation (diet main effect, $P<0.001$, Table 1).

Insulin sensitivity and systemic metabolic function

The LCR rats were more insulin resistant, as indicated by greater HOMA-IR and adipocyte-IR compared to HCR (line main effect, $P<0.001$), and HFD increased HOMA-IR and adipocyte-IR to a greater extent in LCR compared to HCR rats (line × diet interaction, $P=0.001$ and $P=0.004$, respectively; Figure 3A and B). Blood glucose tAUC during GTT was greater following HFD in both lines compared to NC group (diet main effect, $P=0.014$,

Figure 3D). Insulin tAUC during GTT was greater in LCR rats compared to HCR rats (line main effect, P=0.002; Figure 3E). Also, HFD increased insulin secretion during GTT in both lines (diet main effect, P=0.001; Figure 3E). As an additional indicator of skeletal muscle insulin sensitivity, HCR rats showed greater skeletal muscle GLUT4 mRNA expression than LCR rats (line main effect, P<0.001), and HFD reduced GLUT4 mRNA expression in both lines (diet main effect, P<0.001; Figure 3F). Insulin sensitivity calculated using the Matsuda index was significantly attenuated following HFD (diet main effect, P<0.001), and overall HCR rats showed greater insulin sensitivity than LCR rats (line main effect, P=0.001; Table 1). Fasting insulin and glucose levels were significantly higher following HFD compared to the NC group (diet main effect, P=0.007 and P=0.002; Table 1), and LCR rats had greater fasting insulin concentrations than HCR rats (line main effect, P=0.008).

Circulating fasting lipids

LCR rats had higher fasting TG than the HCR (line main effect, P<0.001), and HFD increased TG similarly in HCR and LCR rats (diet main effect, P=0.041; Table 1). NEFA was higher in the LCR than the HCR (line main effect, P=0.006, Table 1), while no significant differences were found in fasting HDL and LDL between lines and diets.

Skeletal muscle AMPK activity

Thr^{172} and $Ser^{485/491}$ of the AMPK α subunit are regarded as the activation and inhibition site for AMPK activity, respectively. HFD significantly attenuated skeletal muscle pAMPK Thr^{172} protein expression in LCR rats but not in HCR rats (line × diet interaction, P=0.044; Figure 4). No significant differences were found between lines and diets in $Ser^{485/491}$ of the AMPK α subunit.

Skeletal muscle mitochondrial biogenesis and content

To assess skeletal muscle mitochondrial biogenesis and content, we measured mRNA expression of the genes, mitochondrial transcription factor A (tFAM), nuclear respiratory factor 1 (NRF1), and peroxisome proliferator-activated receptor γ coactivator 1α (PGC-1α) (Figure 5A). In HFD groups, tFAM mRNA expression was lower compared to the NC groups (diet main effect, P<0.001), and LCR rats exhibited greater reduction with HFD (line × diet interaction, P=0.032). In both lines, HFD reduced NRF1 and PGC-1α mRNA expression (diet main effect, P=0.034 and P=0.015, respectively). Paradoxically, LCR rats showed greater expression of NRF1 and PGC-1α mRNA than HCR rats (line main effect, P=0.003 and P=0.001, respectively). In both lines, HFD reduced CS enzyme activity (diet main effect, P=0.001; Figure 5A), and HCR rats showed greater citrate synthase (CS) activity (line main effect, P=0.003). Overall, HCR rats exhibited greater OX PHOS protein expression than LCR rats (line main effect, P<0.001 in complex I, II, and IV; P=0.037 in complex V, respectively), while HFD attenuated OX PHOS complex proteins similarly in both lines (OX PHOS I, II, IV, and V; diet main effect, P=0.02, 0.004, 0.005, and 0.027, respectively; Figure 5B).

Discussion

Using rats selectively bred for high and low aerobic capacity (HCR, LCR, respectively), the objective of this study was to determine if, following OVX, high aerobic fitness protects against further metabolic dysfunction induced by an HFD. The most salient finding was that, although not protected against HFD-induced increase in adiposity, HCR rats were protected from the development of insulin resistance, unlike the LCR rats. Remarkably, this protection was associated with a compensatory increase in SPA which occurred only in the HCR rats. Previous research has demonstrated that exercise training (11) and aerobic fitness *per se* (39) attenuate OVX-induced metabolic dysfunction in rodents, but the mechanisms have not been fully elucidated. Our group recently demonstrated that HCR rats are protected against OVX-induced insulin resistance and obesity compared to LCR rats (39). In that study, it did not appear that the protection in HCR was due to increased skeletal muscle mitochondrial content in that OVX had no impact on mitochondrial biogenesis markers (i.e. gene and protein content of skeletal muscle PGC1α and oxidative phosphorylation subunits) in either the HCR or LCR. The present study demonstrates that insulin sensitivity and energy expenditure are preserved when HCR_{OVX} rats are exposed to an HFD compared to LCR_{OVX} rats. Interestingly, this protection found in HCR rats is also not linked to their greater skeletal muscle mitochondrial capacity, as HFD decreased those markers similarly in both lines. These novel findings demonstrate that following OVX, 1) despite similar magnitude of weight gain on a HFD, HCR are protected from HFD-induced insulin resistance and reduced TEE compared to LCR, 2) HFD significantly *increases* SPA in HCR and *decrease*s SPA in LCR; this apparent compensatory increase in SPA in HCR likely contributes to the preservation of higher energy expenditure and protection against the development of insulin resistance. Moreover, the increase in SPA in HCR is associated with a maintenance of skeletal muscle AMPK activity which was reduced in LCR; and 3) HFD reduces skeletal muscle mitochondrial biogenesis and content similarly in both lines.

Metabolic dysfunction induced by OVX is associated with ∼90% reduction in circulating levels of sex hormones, comparable to the reduction seen in postmenopausal women (34). Postmenopausal women (3) and OVX rodents (41) develop metabolic dysfunction including increased body weight and adiposity, and may be more susceptible to the negative effects of an HFD. The current study established that, following OVX, both HCR and LCR rats similarly increase body weight gain in the form of adipose tissue in response to an HFD, indicating that high intrinsic aerobic capacity does not provide protection against weight gain under these conditions. Moreover, the accretion of fat mass appeared to result in large part from increased visceral (i.e. perigonadal) adiposity (Figure 1D) which is known to be the depot most closely associated with metabolic dysfunction following loss of ovarian hormones in both rodents and humans. Considerable evidence suggests that expanded adipose tissue and intramuscular lipid accumulation plays a causative role in the development of peripheral insulin resistance (8), which is strongly linked with impaired glucose and lipid disposal pathways (13, 24). Interestingly, although the HCR rats were not impervious to HFD-induced increased adiposity in this current study, they appeared metabolically ‘healthier’ in that they were less fat and insulin resistant than LCR rats following HFD. Specifically, the HFD-induced increase in insulin resistance was greater in

LCR compared to the HCR (HOMA-IR: HCR +190% vs. LCR +580%; adipocyte-IR: HCR +260% vs. LCR +520%; Figure 3A and B). Although no significant interaction was found, many circulating metabolic markers including insulin secretion during GTTs (Figure 3E), circulating TG (Table 1), and GLUT4 gene expression (Figure 3F) indicate that HCR rats are healthier even following HFD compared to LCR rats. Our findings are supported by previous studies using rats with intact ovaries (26, 27) demonstrating that HCR rats are protected against HFD-induced insulin resistance. Further, it appears that the protection from insulin resistance in HCR rats was largely independent of body weight and fat mass. Accordingly, this is the first study to demonstrate that high fitness, independent of total adiposity, protects against metabolic dysfunction associated with loss of ovarian hormones and an HFD.

Previous research (10, 18) has reported that HFD-induced weight gain results from increased energy intake due to the high energy density of HFD. However, in the present study, no increase in total energy consumption occurred with HFD feeding in either line. Thus, both lines compensated for the high energy density of the HFD by reducing the amount of food they consumed. Moreover, neither line differed in their body weight-relative energy intake on control diet (Figure 2D).

In addition to a protective effect of high aerobic capacity in HFD-induced insulin resistance, another notable finding in the present study is that HCR are resistant to HFD-induced reduction in TEE during the dark cycle found in LCR (Figure 2A). Interestingly, SPA in the dark cycle is altered differentially in HCR and LCR rats with exposure to HFD feeding; HFD increased SPA in the HCR and decreased it in the LCR. Considering the fact that REE was reduced following HFD in HCR (Figure 2C), it appears that a compensatory increase in SPA contributes to the preserved TEE following HFD in HCR rats, and also likely explains the protection against HFD-induced insulin resistance in HCR rats. This interesting phenomenon of differential activity pattern in response to HFD in a HCR/LCR model has been reported earlier by Noland et al. (27) and by a study using a different model of obesity-resistant vs. -prone rats (28), indicating the significant role of a compensatory increase in SPA levels to attenuate the consequence of external metabolic stress (e.g. HFD) in terms of obesity and insulin resistance. Conversely, other studies (17, 25) have also shown that the differences in weight gain and obesity between obesity-resistant and -prone rats are not associated with the different SPA responses to a HFD. Our finding with skeletal muscle AMPK activity supports the compensatory increase in SPA found in HCR rats. pAMPK Thr^{172} (activation site) expression in skeletal muscle was maintained following HFD feeding in HCR, while it decreased in LCR (Figure 4A). We speculate that, in HCR rats, increased SPA protects against the HFD-induced reduction in pAMPK Thr^{172} found in LCR, as it has been established that increased physical activity upregulates AMPK activity (32). AMPK has been extensively studied as a major regulator of many cellular pathways including oxidative metabolism (7). OVX is accompanied by diminished estrogenic signaling and AMPK activity in skeletal muscle (14). In the present study, it is unknown if OVX *per se* affects AMPK activity in our HCR/LCR model, as all rats were OVX. However, it is obvious that a HFD administration would be a strong external factor to diminish AMPK activity in LCR rats when sex hormones including estrogen are depleted by OVX, and this AMPK change paralleled aggravated insulin resistance. A previous study (20) in ovary-intact rats

demonstrated that HFD substantially attenuates isoforms of AMPK in multiple tissues and exert systemic insulin resistance. Taken together, we speculate that an HFD attenuates AMPK activity independent of ovarian hormone production, and that enhanced SPA may protect against this diminished AMPK activity in HCR rats. Although the current investigation does not provide a clear underlying molecular mechanism by the differential SPA response to HFD between HCR and LCR rats, the present data offers sufficient evidence to warrant further investigations.

REE accounts for the majority of TEE (∼ 70%) in caged rodents, while physical activity energy expenditure accounts for ∼20-25% of TEE (31). Although we found that HCR are protected from HFD-induced reduction in TEE via increased SPA, REE in both dark and light cycles was reduced following HFD in both lines (dark: HCR -7% vs. LCR -9%; light: HCR -5% vs. LCR -10%). This finding varies from those of previous studies. Vaanholt et al. (38) initially reported that mice selectively bred for high wheel-running activity were protected from HFD-induced obesity; this protection was likely due to the compensatory increase in REE following a HFD. This phenomenon has been shown in our HCR/LCR model without OVX (9, 25). In a study by Morris et al. (25), REE was maintained following an HFD in HCR after adjusting for body weight. Also, HCR are partially protected from the OVX-associated reduction in REE and insulin resistance apparent in LCR (39). It may be that it is the failure of a compensatory increase in (or maintenance of) REE in response to HFD that results in increased adiposity. In the present study, following OVX, HFD appears to be a strong contributor to reduce REE even in HCR rats.

We have previously demonstrated that skeletal muscle mitochondrial markers, including PGC-1α and some oxidative phosphorylation complexes are greater in ovary-intact HCR rats compared to ovary-intact LCR rats (39). However, in that study, we found no indication that these markers were affected by OVX in either line, suggesting that modifications of skeletal muscle mitochondrial biogenesis and content were not mechanistically related to the protection against OVX-induced insulin resistance and obesity in HCR. In the present study, due to evidence that HFD feeding induces skeletal muscle insulin resistance and, in some cases, reduces mitochondrial biogenesis and function in rodent models (4, 35), we sought to determine if these mitochondrial markers are differentially affected by a HFD in HCR_{OVX} and LCR_{OVX} rats. We hypothesized that HCR rats would be protected from HFD-induced reductions in skeletal muscle mitochondrial oxidative capacity. Our results showed that, despite a compensatory increase in SPA in the HCR, a HFD reduces markers of mitochondrial biogenesis and content similarly in both lines. However, in most conditions, the HCR have greater abundance of those markers than LCR. Attenuated expression of transcription factors (i.e. PGC-1α, NRF1, and tFAM) regulating mitochondrial biogenesis and oxidative phosphorylation in skeletal muscle are putatively linked to insulin sensitivity and T2D (19, 30). The present study reveals that skeletal muscle gene expression of PGC-1α and NRF1 are down regulated following a HFD but, paradoxically, those genes are expressed at a higher level in LCR (Figure 5A). This may imply a compensatory increase in transcription to counter the lower mitochondrial content in this line; it is also possible that posttranslational modification (e.g., protein ubiquitination and degradation) resulted in no protein differences between lines (6). In line with this idea, protein expression of oxidative phosphorylation complexes (complex I, II, IV and V) and CS enzyme activity were lower in

LCR compared to HCR (Figure 5A and B). Even though HCR have greater protein expression of skeletal muscle oxidative phosphorylation markers compared to LCR, HFD decreased those markers even in HCR rats. HFD also significantly affected skeletal muscle gene expression (e.g., reduced estrogen receptor (ERα)) in both HCR and LCR rats (see Figure, Supplemental Digital Content 1, which demonstrates relative mRNA expression of genes related to skeletal muscle metabolism, estrogen signaling, inflammation, and oxidative stress in gastrocnemeous muscle samples from HCR and LCR rats fed HFD vs. NC). However, this HFD-induced reduction in mitochondrial biogenesis markers was observed despite maintained AMPK activity in HCR, whereas this was not the case with LCR. This finding is in contrast with previous research (2) showing a significant relationship between AMPK and mitochondrial capacity. Little is known about the role of AMPK on regulating oxidative metabolism during a loss of ovarian hormones.

A limitation of the study is that the rats were not ovariectomized at an older stage in development (i.e., ∼ 1-2 years). Given that human menopause involves both aging and loss of ovarian hormones, an ideal rodent model will exemplify both traits. We performed OVX surgeries at ∼ 30 weeks, which would be considered mature adult. The mature adult rodent OVX model may be considered a good model of human menopause in that it displays the constellation of metabolic symptoms observed in human menopause. Moreover, it allows for investigation of the effects of loss of ovarian hormones without the potential confounding factor of aging. Future studies are needed to determine how aging *per se* might impact the outcomes reported in this present study. Another limitation is that, although a subset of mRNA samples used to generate gene expression differences were tested for quality assurance (i.e., via RNA quality number (RQN) determination), we did not test each sample. However, each one of the randomly-selected samples tested with optimal RQNs. Along those lines, we did not determine the linear dynamic range for each protein and gene measured along side the respective control genes/proteins. Thus, those molecular analyses should be viewed in light of those methodological limitations.

In summary, high intrinsic aerobic capacity (i.e. HCR rats) is protective against HFD-associated metabolic dysfunction in the OVX condition. In contrast to our initial hypothesis that an underlying mechanism by which HCR_{OVX} rats are protected from HFD-induced metabolic dysfunction is preservation of skeletal muscle mitochondrial biogenesis and content, HCR appear to be protected from HFD-associated insulin resistance through a unique mechanism of behavioral change. The apparent compensatory increase in SPA in HCR relates strongly to their preservation of TEE and skeletal muscle AMPK activity; this protective effect is independent of REE and skeletal muscle mitochondrial biogenesis and content. In conclusion, following OVX, high intrinsic aerobic capacity rats are resistant to HFD-associated insulin resistance and reduction in TEE likely via increased SPA.

Supplementary Material

Refer to Web version on PubMed Central for supplementary material.

Acknowledgments

This research was supported by MU Research Council grant (VVP), NIH K01HL125503 (JP), R01DK088940 (JPT), R24OD010950 (LGK and SLB), R01DK077200 and R01GM104194 (SLB).

References

1. Booth FW, Laye MJ, Roberts MD. Lifetime sedentary living accelerates some aspects of secondary aging. J Appl Physiol. 1985; 111(5):1497–504. [PubMed: 21836048]
2. Canto C, Auwerx J. PGC-1alpha, SIRT1 and AMPK, an energy sensing network that controls energy expenditure. Current opinion in lipidology. 2009; 20(2):98–105. [PubMed: 19276888]
3. Carr MC. The emergence of the metabolic syndrome with menopause. The Journal of clinical endocrinology and metabolism. 2003; 88(6):2404–11. [PubMed: 12788835]
4. Coen PM, Goodpaster BH. Role of intramyocelluar lipids in human health. Trends in endocrinology and metabolism: TEM. 2012; 23(8):391–8. [PubMed: 22721584]
5. Earnest CP, Johannsen NM, Swift DL, Lavie CJ, Blair SN, Church TS. Dose effect of cardiorespiratory exercise on metabolic syndrome in postmenopausal women. The American journal of cardiology. 2013; 111(12):1805–11. [PubMed: 23578351]
6. Fernandez-Marcos PJ, Auwerx J. Regulation of PGC-1alpha, a nodal regulator of mitochondrial biogenesis. The American journal of clinical nutrition. 2011; 93(4):884S–90. [PubMed: 21289221]
7. Hardie DG. AMP-activated protein kinase: an energy sensor that regulates all aspects of cell function. Genes & development. 2011; 25(18):1895–908. [PubMed: 21937710]
8. Hulver MW, Dohm GL. The molecular mechanism linking muscle fat accumulation to insulin resistance. The Proceedings of the Nutrition Society. 2004; 63(2):375–80. [PubMed: 15294058]
9. Jackman MR, MacLean PS, Bessesen DH. Energy expenditure in obesity-prone and obesity-resistant rats before and after the introduction of a high-fat diet. American journal of physiology Regulatory, integrative and comparative physiology. 2010; 299(4):R1097–105.
10. Jang I, Hwang D, Lee J, et al. Physiological difference between dietary obesity-susceptible and obesity-resistant Sprague Dawley rats in response to moderate high fat diet. Experimental animals / Japanese Association for Laboratory Animal Science. 2003; 52(2):99–107. [PubMed: 12806884]
11. Jeong S, Yoon M. Swimming's prevention of ovariectomy-induced obesity through activation of skeletal-muscle PPARalpha. International journal of sport nutrition and exercise metabolism. 2012; 22(1):1–10. [PubMed: 22248494]
12. Johnson ML, Ho CC, Day AE, Walker QD, Francis R, Kuhn CM. Oestrogen receptors enhance dopamine neurone survival in rat midbrain. Journal of neuroendocrinology. 2010; 22(4):226–37. [PubMed: 20136693]
13. Kelley DE, He J, Menshikova EV, Ritov VB. Dysfunction of mitochondria in human skeletal muscle in type 2 diabetes. Diabetes. 2002; 51(10):2944–50. [PubMed: 12351431]
14. Kim JY, Jo KJ, Kim OS, et al. Parenteral 17beta-estradiol decreases fasting blood glucose levels in non-obese mice with short-term ovariectomy. Life sciences. 2010; 87(11-12):358–66. [PubMed: 20655933]
15. Koch LG, Britton SL. Artificial selection for intrinsic aerobic endurance running capacity in rats. Physiological genomics. 2001; 5(1):45–52. [PubMed: 11161005]
16. Kodama S, Saito K, Tanaka S, et al. Cardiorespiratory fitness as a quantitative predictor of all-cause mortality and cardiovascular events in healthy men and women: a meta-analysis. JAMA : the journal of the American Medical Association. 2009; 301(19):2024–35. [PubMed: 19454641]
17. Levin BE. Spontaneous motor activity during the development and maintenance of diet-induced obesity in the rat. Physiology & behavior. 1991; 50(3):573–81. [PubMed: 1801012]
18. Levin BE, Triscari J, Hogan S, Sullivan AC. Resistance to diet-induced obesity: food intake, pancreatic sympathetic tone, and insulin. The American journal of physiology. 1987; 252(3 Pt 2):R471–8. [PubMed: 3548441]
19. Lin J, Handschin C, Spiegelman BM. Metabolic control through the PGC-1 family of transcription coactivators. Cell metabolism. 2005; 1(6):361–70. [PubMed: 16054085]

20. Lindholm CR, Ertel RL, Bauwens JD, Schmuck EG, Mulligan JD, Saupe KW. A high-fat diet decreases AMPK activity in multiple tissues in the absence of hyperglycemia or systemic inflammation in rats. Journal of physiology and biochemistry. 2013; 69(2):165–75. [PubMed: 22941749]
21. Manson JE, Greenland P, LaCroix AZ, et al. Walking compared with vigorous exercise for the prevention of cardiovascular events in women. The New England journal of medicine. 2002; 347(10):716–25. [PubMed: 12213942]
22. Matsuda M, DeFronzo RA. Insulin sensitivity indices obtained from oral glucose tolerance testing: comparison with the euglycemic insulin clamp. Diabetes care. 1999; 22(9):1462–70. [PubMed: 10480510]
23. Matthews DR, Hosker JP, Rudenski AS, Naylor BA, Treacher DF, Turner RC. Homeostasis model assessment: insulin resistance and beta-cell function from fasting plasma glucose and insulin concentrations in man. Diabetologia. 1985; 28(7):412–9. [PubMed: 3899825]
24. Mootha VK, Lindgren CM, Eriksson KF, et al. PGC-1alpha-responsive genes involved in oxidative phosphorylation are coordinately downregulated in human diabetes. Nature genetics. 2003; 34(3): 267–73. [PubMed: 12808457]
25. Morris EM, Jackman MR, Johnson GC, et al. Intrinsic aerobic capacity impacts susceptibility to acute high-fat diet-induced hepatic steatosis. American journal of physiology Endocrinology and metabolism. 2014; 307(4):E355–64. [PubMed: 24961240]
26. Naples SP, Borengasser SJ, Rector RS, et al. Skeletal muscle mitochondrial and metabolic responses to a high-fat diet in female rats bred for high and low aerobic capacity. Applied physiology, nutrition, and metabolism = Physiologie appliquee, nutrition et metabolisme. 2010; 35(2):151–62.
27. Noland RC, Thyfault JP, Henes ST, et al. Artificial selection for high-capacity endurance running is protective against high-fat diet-induced insulin resistance. American journal of physiology Endocrinology and metabolism. 2007; 293(1):E31–41. [PubMed: 17341547]
28. Novak CM, Kotz CM, Levine JA. Central orexin sensitivity, physical activity, and obesity in diet-induced obese and diet-resistant rats. American journal of physiology Endocrinology and metabolism. 2006; 290(2):E396–403. [PubMed: 16188908]
29. Padilla J, Jenkins NT, Vieira-Potter VJ, Laughlin MH. Divergent phenotype of rat thoracic and abdominal perivascular adipose tissues. American journal of physiology Regulatory, integrative and comparative physiology. 2013; 304(7):R543–52.
30. Patti ME, Butte AJ, Crunkhorn S, et al. Coordinated reduction of genes of oxidative metabolism in humans with insulin resistance and diabetes: Potential role of PGC1 and NRF1. Proceedings of the National Academy of Sciences of the United States of America. 2003; 100(14):8466–71. [PubMed: 12832613]
31. Poehlman ET. A review: exercise and its influence on resting energy metabolism in man. Medicine and science in sports and exercise. 1989; 21(5):515–25. [PubMed: 2691813]
32. Ruderman NB, Carling D, Prentki M, Cacicedo JM. AMPK, insulin resistance, and the metabolic syndrome. The Journal of clinical investigation. 2013; 123(7):2764–72. [PubMed: 23863634]
33. Seifert EL, Bastianelli M, Aguer C, et al. Intrinsic aerobic capacity correlates with greater inherent mitochondrial oxidative and H2O2 emission capacities without major shifts in myosin heavy chain isoform. J Appl Physiol (1985). 2012; 113(10):1624–34. [PubMed: 22995392]
34. Spangenburg EE, Wohlers LM, Valencia AP. Metabolic dysfunction under reduced estrogen levels: looking to exercise for prevention. Exercise and sport sciences reviews. 2012; 40(4):195–203. [PubMed: 22653278]
35. Sparks LM, Xie H, Koza RA, et al. A high-fat diet coordinately downregulates genes required for mitochondrial oxidative phosphorylation in skeletal muscle. Diabetes. 2005; 54(7):1926–33. [PubMed: 15983191]
36. Srere PA. Citrate synthase. Methods in Enzymology. 1969; 13:3–11.
37. Thyfault JP, Rector RS, Uptergrove GM, et al. Rats selectively bred for low aerobic capacity have reduced hepatic mitochondrial oxidative capacity and susceptibility to hepatic steatosis and injury. The Journal of physiology. 2009; 587(Pt 8):1805–16. [PubMed: 19237421]

38. Vaanholt LM, Jonas I, Doornbos M, et al. Metabolic and behavioral responses to high-fat feeding in mice selectively bred for high wheel-running activity. Int J Obes (Lond). 2008; 32(10):1566–75. [PubMed: 18725891]

39. Vieira-Potter VJ, Padilla J, Park YM, et al. Female Rats Selectively Bred for High Intrinsic Aerobic Fitness Are Protected from Ovariectomy-Associated Metabolic Dysfunction. American journal of physiology Regulatory, integrative and comparative physiology. 2015 ajpregu 00401 2014.

40. Wisloff U, Najjar SM, Ellingsen O, et al. Cardiovascular risk factors emerge after artificial selection for low aerobic capacity. Science. 2005; 307(5708):418–20. [PubMed: 15662013]

41. Yonezawa R, Wada T, Matsumoto N, et al. Central versus peripheral impact of estradiol on the impaired glucose metabolism in ovariectomized mice on a high-fat diet. American journal of physiology Endocrinology and metabolism. 2012; 303(4):E445–56. [PubMed: 22550066]

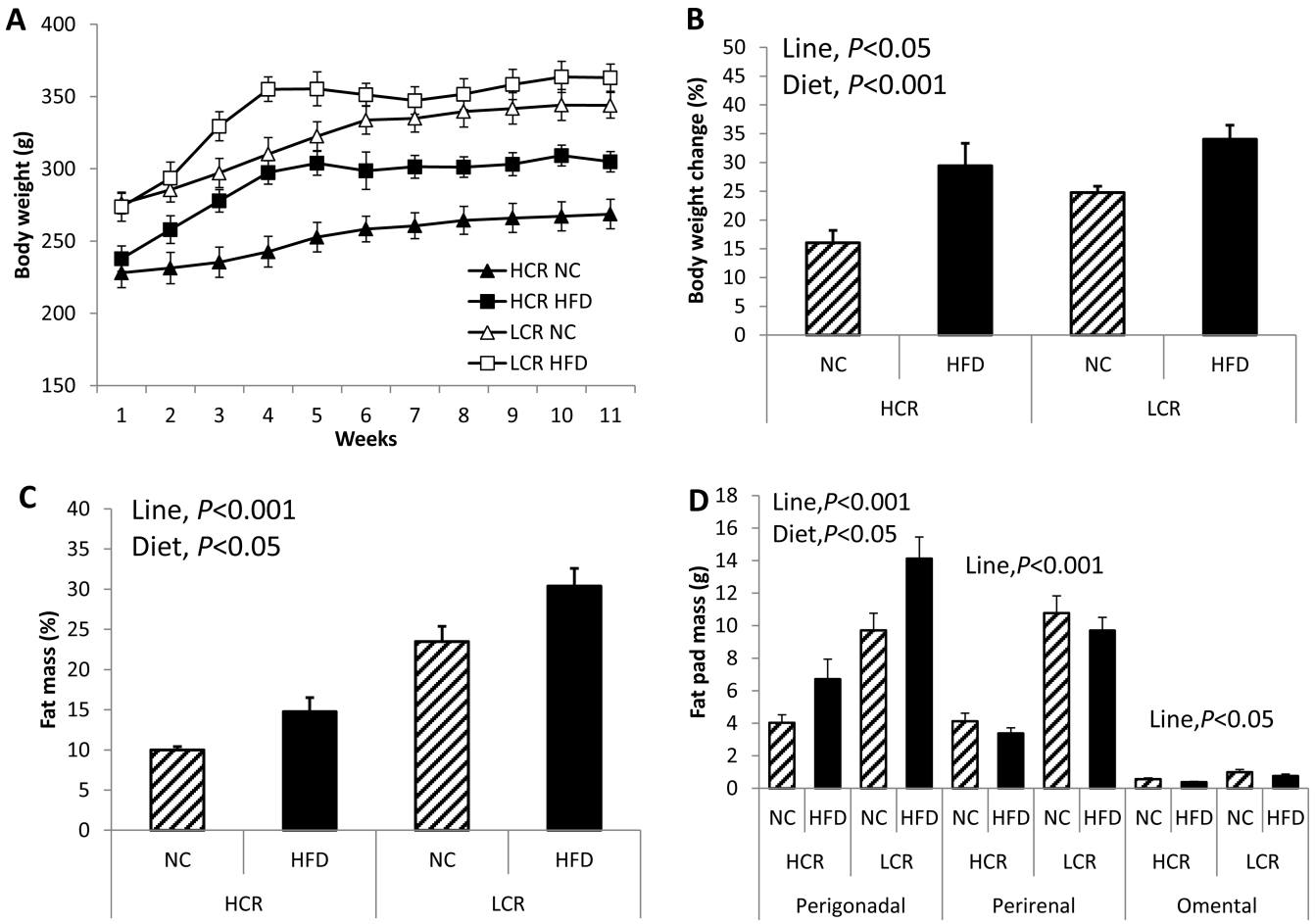

Figure 1. Despite OVX LCR being significantly fatter than OVX HCR, both lines display increased fat pad weights with a HFD

(A) Body weight gain curves for 11 weeks, (B) total % body weight gain from baseline, (C) % body fat via DXA analysis, and (D) adipose tissue distribution via visceral fat pad mass. Values are means ± SE (n=7-12 per group). Line = line main effect, HCR vs. LCR; Diet = diet main effect, NC vs. HFD.

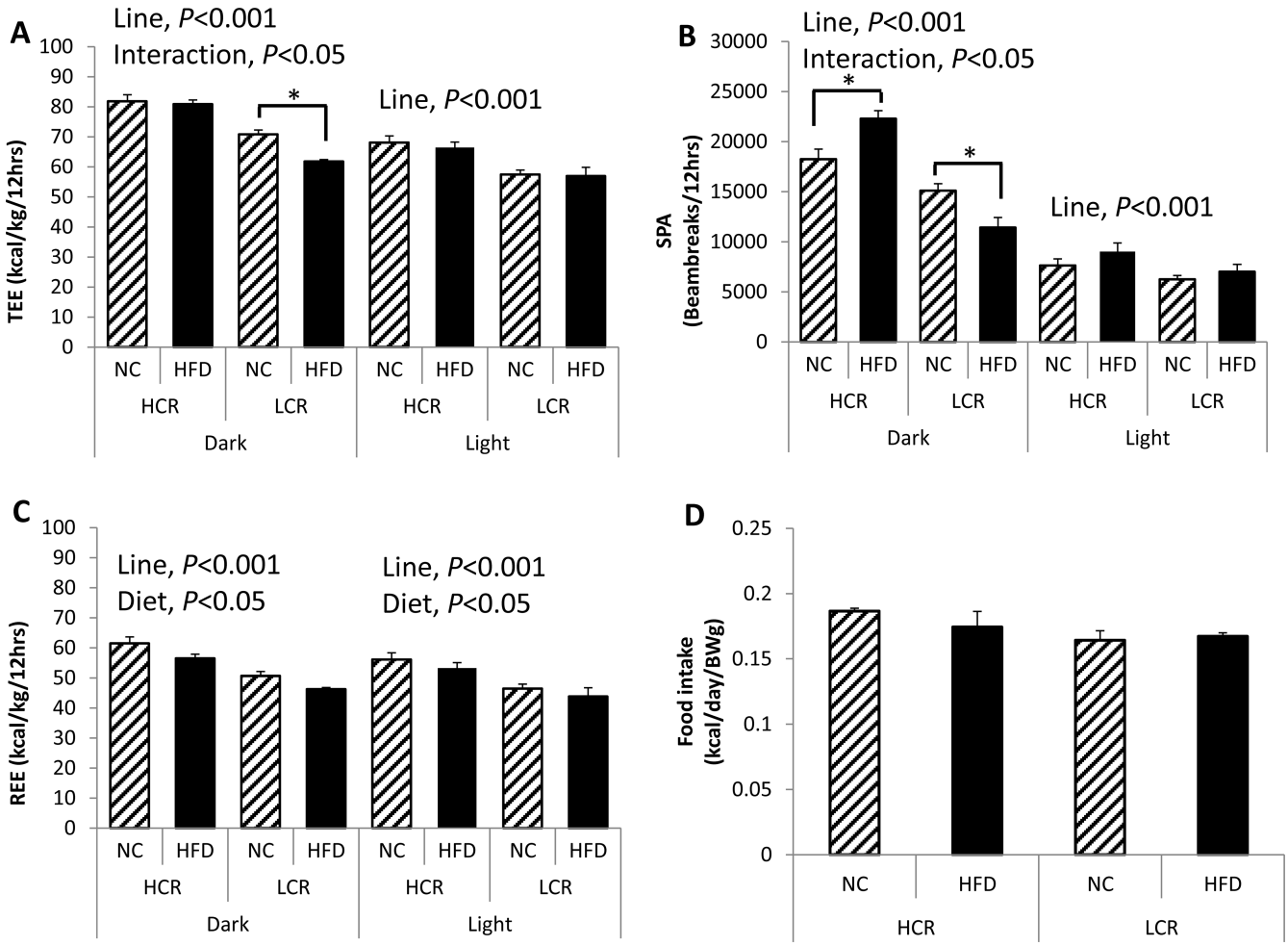

Figure 2. HCR are protected against HFD-induced reduction in energy expenditure putatively via enhanced spontaneous physical activity

(A) total energy expenditure (TEE), (B) spontaneous physical activity (SPA), (C) resting energy expenditure (REE), and (D) food intake relative to body weight. Values are means ± SE (n=5-6 per group). Line = line main effect, HCR vs. LCR; Diet = diet main effect, NC vs. HFD; Interaction = line × diet interaction. * Denotes difference (P<0.05) between NC and HFD within line.

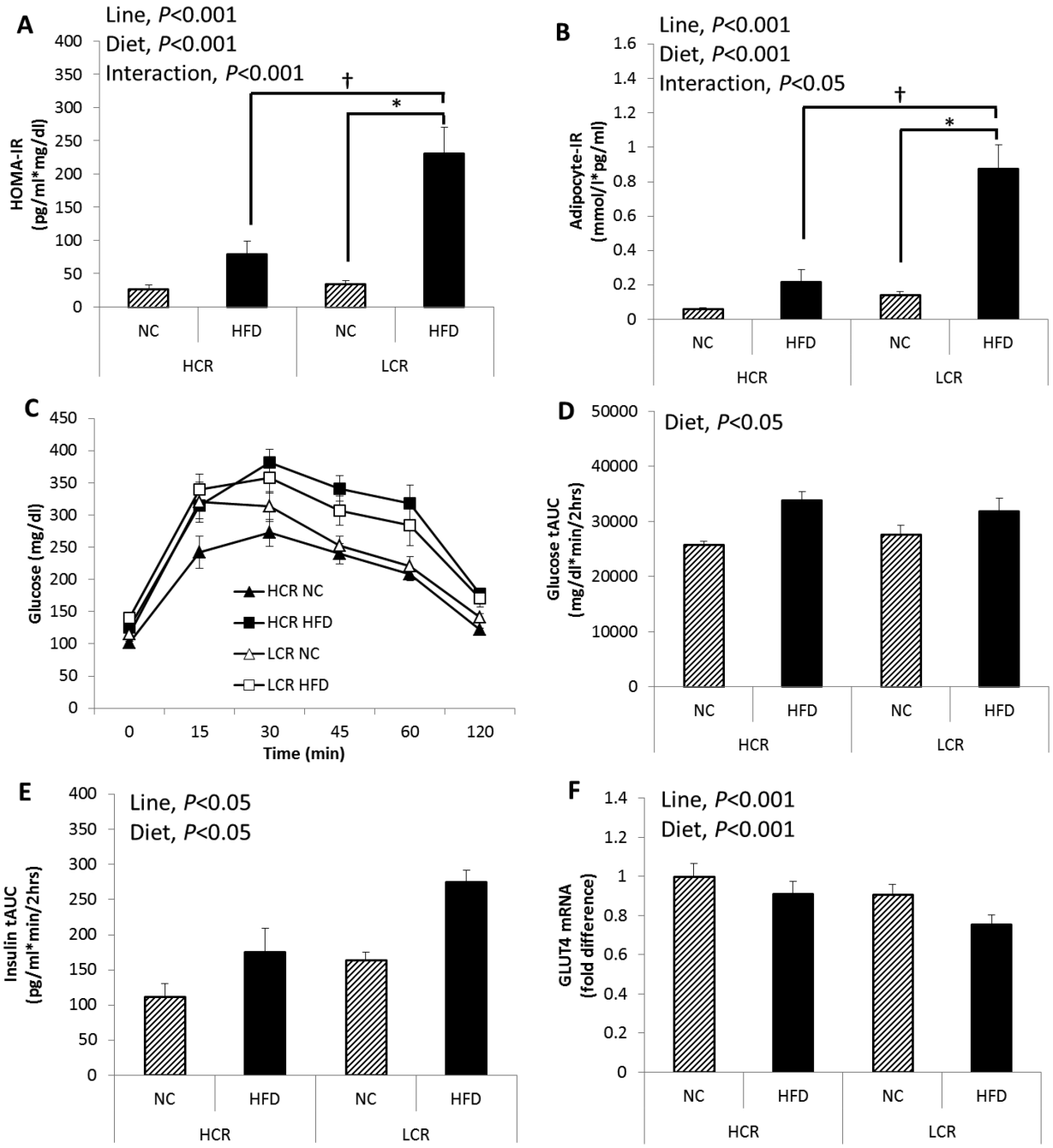

Figure 3. Despite similar weight gain on HFD, HCR are partially protected against HFD-induced insulin resistance

(A) HOMA-IR, (B) adipocyte-IR, (C) plasma glucose levels during a 2-hour intraperitoneal glucose tolerance test (GTT), (D) glucose tAUC during GTT, (E) Insulin secretion during GTT indicated as insulin tAUC, and (F) skeletal muscle glucose transporter type 4 (GLUT4) mRNA expression. Values are means ± SE (n=5-6 per group). Line = line main effect, HCR vs. LCR; Diet = diet main effect, NC vs. HFD; Interaction = line × diet interaction. * Denotes difference (P<0.05) between NC and HFD within line. † Denotes difference (P<0.05) between HCR HFD and LCR HFD.

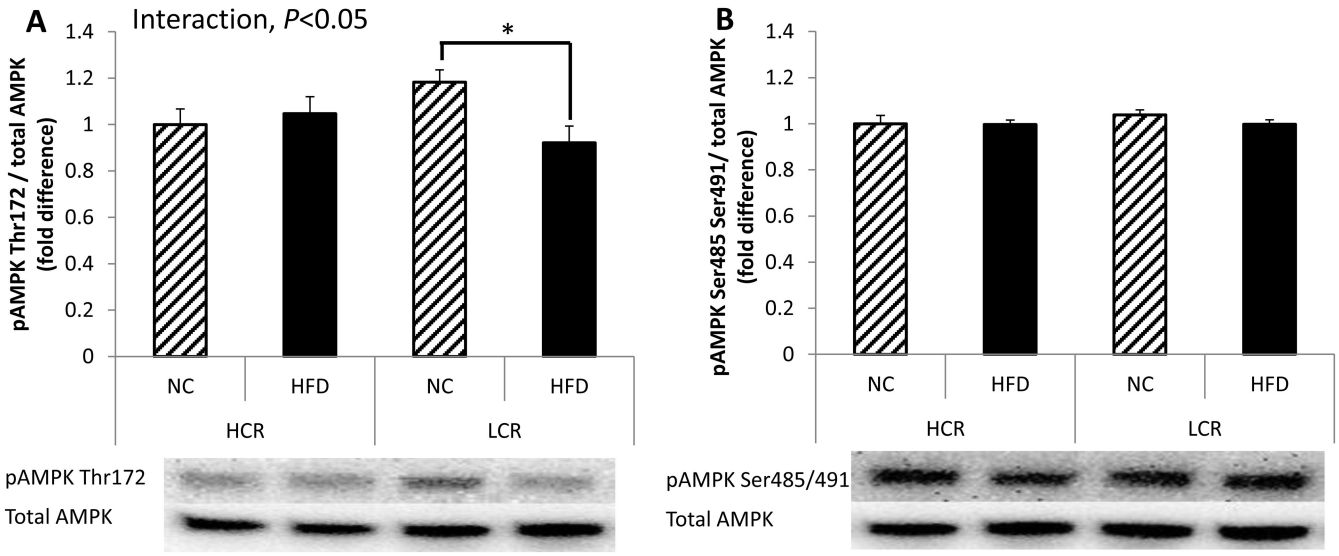

Figure 4. HCR are protected from HFD-associated reduction in skeletal muscle AMPK activity

(A) pAMPK Thr^{172} (activation site) and (B) pAMPK Ser$^{485/491}$ (inhibition site). Values are normalized by total AMPK; values are means ± SE (n=6-9 per group). Interaction = line × diet interaction. * Denotes difference (P<0.05) between NC and HFD within line.

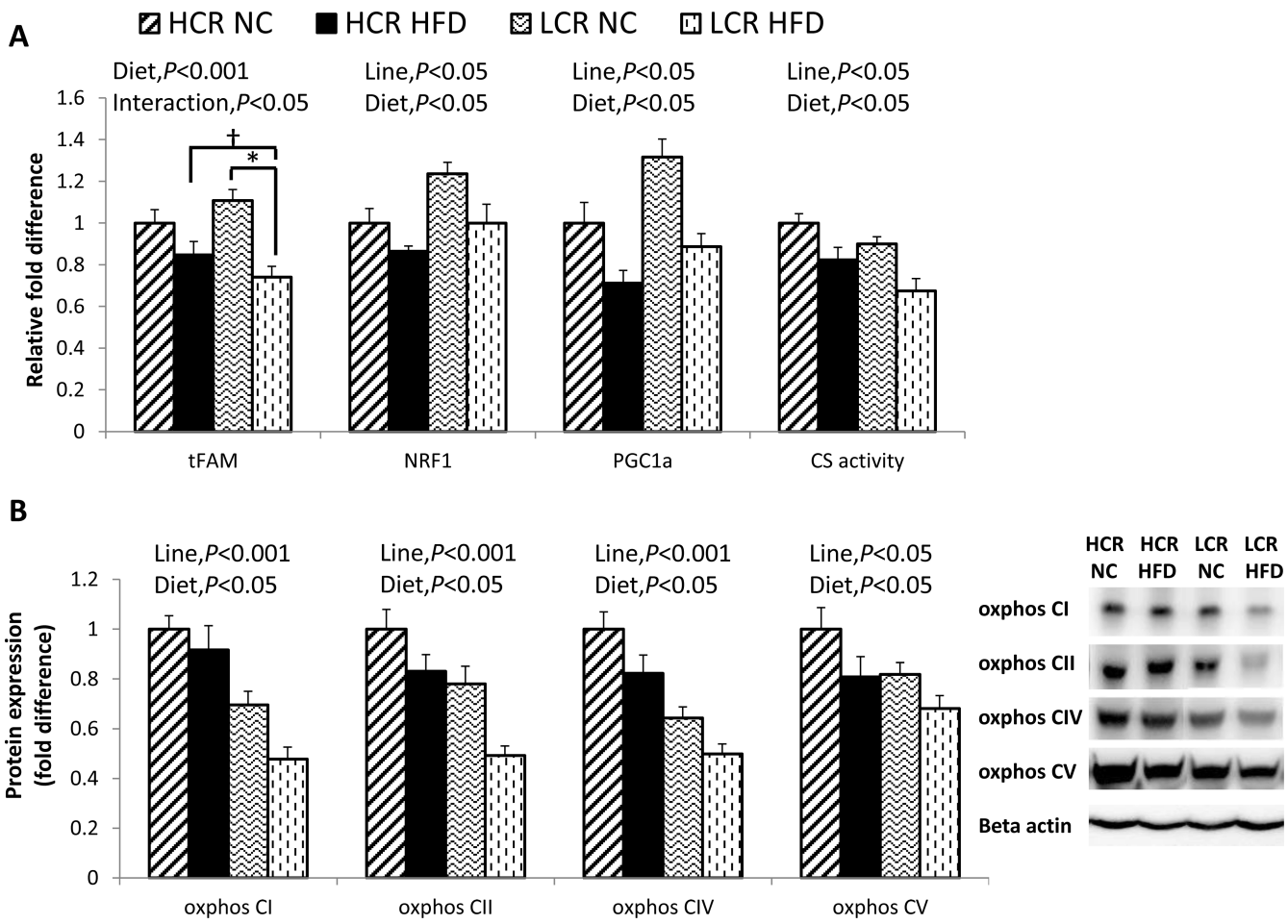

Figure 5. HFD reduces skeletal muscle mitochondrial biogenesis and content in both lines

(A) skeletal muscle mRNA expressions for mitochondrial transcription factor A (tFAM), nuclear respiratory factor 1 (NRF1), and peroxisome proliferator-activated receptor γ coactivator 1α (PGC-1α); skeletal muscle citrate synthase (CS) enzyme activity; (B) oxidative phosphorylation (OX PHOS) complex I, II, IV, and V proteins in skeletal muscle. Values are means ± SE (n=7-10 per group). Line = line main effect, HCR vs. LCR; Diet = diet main effect, NC vs. HFD; Interaction = line × diet interaction. * Denotes difference (*P*<0.05) between NC and HFD within line. † Denotes difference (*P*<0.05) between HCR HFD and LCR HFD.

Table 1

Body composition and metabolic characteristics

	HCR		LCR		2-way ANOVA statistics
	NC	HFD	NC	HFD	
Initial body weight (g)	228.08 ± 10.24	237.94 ± 8.79	275.99 ± 7.14	273.82 ± 10.08	Line, P<0.001
Final body weight (g)	264.01 ± 10.53	306.52 ± 8.37	344.66 ± 10.23	366.24 ± 11.17	Line, P<0.001 Diet, P=0.005
Final lean mass (g)	241.30 ± 11.53	266.97 ± 7.35	263.19 ± 9.02	254.75 ± 10.68	NS
Heart (g/BWg)	0.0038 ± 0.00024	0.0030 ± 0.00006	0.0030 ± 0.00016	0.0027 ± 0.00012	Line, P=0.002 Diet, P=0.002
BAT/WAT (g/g)	0.037 ± 0.003	0.030 ± 0.004	0.014 ± 0.002	0.014 ± 0.002	Line, P<0.001
Liver (g)	7.28 ± 0.53	6.67 ± 0.54	7.81 ± 0.37	6.71 ± 0.23	NS
TG (mg/dL)	25.28 ± 2.37	32.71 ± 5.29	42.71 ± 2.82	52.00 ± 4.78	Line, P<0.001 Diet, P=0.041
NEFA (mmol/L)	0.29 ± 0.05	0.31 ± 0.05	0.46 ± 0.02	0.45 ± 0.04	Line, P=0.006
HDL (mg/dL)	29.75 ± 2.01	24.42 ± 1.34	30.46 ± 2.07	30.35 ± 1.31	NS
LDL (mg/dL)	2.8 ± 0.29	2.28 ± 0.18	2.20 ± 0.12	3.21 ± 0.26	NS
Insulin (pg/mL)	0.27 ± 0.05	0.60 ± 0.13	0.59 ± 0.21	1.65 ± 0.27	Line, P=0.008 Diet, P=0.007
Glucose (mg/dL)	99.8 ± 2.5	126.0 ± 8.1	113.4 ± 6.1	139.8 ± 7.4	Line, P=0.084 (NS) Diet, P=0.002
Uterine (g)	0.299 ± 0.052	0.261 ± 0.027	0.263 ± 0.043	0.289 ± 0.017	NS
IS (Matsuda index)	15.15 ± 1.29	6.84 ± 1.42	8.39 ± 0.80	2.79 ± 0.32	Line, P=0.001 Diet, P<0.001
RQ (dark cycle)	0.93 ± 0.01	0.74 ± 0.02	0.91 ± 0.01	0.77 ± 0.01	Diet, P<0.001
RQ (light cycle)	0.92 ± 0.01	0.73 ± 0.02	0.88 ± 0.01	0.75 ± 0.01	Diet, P<0.001
SPA (x + y, dark)	9629.2 ± 836.5	13230.8 ± 690.5	7173.3 ± 549.5	6383.3 ± 942.4	Line, P<0.001 Diet, P=0.161(NS) Interaction, P=0.035
SPA (x + y, light)	3639.9 ± 473.7	5632.2 ± 303.3	3076.7 ± 343.7	3263.3 ± 458.4	Line, P=0.011 Diet, P=0.049 Interaction, P=0.097 (NS)
Pedmeters (meter, dark)	80.48 ± 9.48	130.35 ± 12.57	74.97 ± 9.57	55.57 ± 6.51	Line, P=0.02 Diet, P=0.170 (NS) Interaction, P=0.005
Pedmeters (meter, light)	26.82 ± 3.71	65.10 ± 5.74	34.07 ± 5.73	32.08 ± 9.69	Line, P=0.139 (NS) Diet, P=0.007 Interaction, P=0.018